Discovery of a Novel Inhibitor of Human Purine Nucleoside Phosphorylase by a Simple Hydrophilic Interaction Liquid Chromatography Enzymatic Assay

Marco Rabuffetti[+],[a] Francesca Rinaldi[+],[b] Alessandra Lo Bianco[+],[c] Giovanna Speranza,[a] Daniela Ubiali,[b] Marcela Cristina de Moraes,[d] Luiz Claudio Rodrigues Pereira da Silva,[e] Gabriella Massolini,[b] Enrica Calleri,*[b] and Antonio Lavecchia*[c]

Human purine nucleoside phosphorylase (*Hs*PNP) belongs to the purine salvage pathway of nucleic acids. Genetic deficiency of this enzyme triggers apoptosis of activated T-cells due to the accumulation of deoxyguanosine triphosphate (dGTP). Therefore, potential chemotherapeutic applications of human PNP inhibitors include the treatment of T-cell leukemia, autoimmune diseases and transplant tissue rejection. In this report, we present the discovery of novel *Hs*PNP inhibitors by coupling experimental and computational tools. A simple, inexpensive, direct and non-radioactive enzymatic assay coupled to hydrophilic interaction liquid chromatography and UV detection (LC-UV using HILIC as elution mode) was developed for screening *Hs*PNP inhibitors. Enzymatic activity was assessed by monitoring the phosphorolysis of inosine (Ino) to hypoxanthine (Hpx) by LC-UV. A small library of 6- and 8-substituted nucleosides was synthesized and screened. The inhibition potency of the most promising compound, 8-aminoinosine (**4**), was quantified through K_i and IC_{50} determinations. The effect of *Hs*PNP inhibition was also evaluated *in vitro* through the study of cytotoxicity on human T-cell leukemia cells (CCRF-CEM). Docking studies were also carried out for the most potent compound, allowing further insights into the inhibitor interaction at the *Hs*PNP active site. This study provides both new tools and a new lead for developing novel *Hs*PNP inhibitors.

Introduction

Purine nucleoside phosphorylases (PNPs) are multimeric enzymes that catalyze the reversible cleavage of the glycosidic bond of purine ribonucleosides and deoxyribonucleosides in presence of inorganic orthophosphate (P_i) as a second substrate to generate the corresponding purine nucleobase and α-D-(deoxy)ribose-1-phosphate.[1] In the absence of human PNP (*Hs*PNP), nucleoside substrates, such as 2′-deoxyguanosine (dGuo), accumulate.[2] The accumulation of dGuo has been observed in children with an inherited PNP deficiency. These children exhibit severe T-cell immunodeficiency, but retain normal B-cell function. Phosphorylation of dGuo (by 2′-deoxycytidine kinase, dCK) to 2′-deoxyguanosine triphosphate (dGTP) is responsible for T-cell cytotoxicity. dGTP allosterically inhibits the enzyme ribonucleoside-5′-diphosphate reductase, impairing DNA synthesis and initiating T-cell apoptosis.[3] Human T-cells are unique in that they display a combination of high dCK activity and relatively low nucleotidase activity, which allows these cells to accumulate dGTP.[4] Therefore, *Hs*PNP is considered an attractive chemotherapeutic target for T-cell proliferative disorders, such as psoriasis, multiple sclerosis, rheumatoid arthritis, organ transplant rejection and inflammatory bowel disorders.[5] Additionally, T-cell leukemias and lymphomas would be primary proliferative targets for PNP inhibitors.[6] PNP inhibitors have been also studied due to their ability to enhance the activity of antiviral and anticancer nucleoside drugs.[7]

The first inhibitors of PNP were developed using structure-based inhibitor design focused on iterative group alignment established from the PNP crystal structure.[8] The bound-substrate transition state structure of *Hs*PNP has subsequently permitted the design of several transition state analogues with picomolar dissociation constants.[6a,9] Four structurally distinct generations of transition state analogues have been synthesized (Figure 1). The first-generation inhibitor, Immucillin-H (clinically Forodesine and Mundesine), designed to mimic the early dissociative transition state of bovine PNP,[10] has been approved in Japan for the treatment of resistant and relapsed peripheral T-cell lymphoma. Immucillin-H [(1*S*)-1-(9-deazahypoxanthin-9-yl)-1,4-dideoxy-1,4-imino-D-ribitol] binds with a K_d of 23 pM to the bovine enzyme and with a slightly higher K_d of

[a] *Dr. M. Rabuffetti,[+] Prof. G. Speranza*
Department of Chemistry, University of Milan
Via Golgi 21, 20133 Milan (Italy)
[b] *Dr. F. Rinaldi,[+] Prof. D. Ubiali, Prof. G. Massolini, Prof. E. Calleri*
Department of Drug Sciences, University of Pavia
Viale Taramelli 12, 27100 Pavia (Italy)
E-mail: enrica.calleri@unipv.it
[c] *Dr. A. Lo Bianco,[+] Prof. A. Lavecchia*
Department of Pharmacy, "Drug Discovery" Laboratory
University of Napoli Federico II
Via D. Montesano 49, 80131 Napoli (Italy)
E-mail: antonio.lavecchia@unina.it
[d] *Prof. M. C. de Moraes*
Departamento de Química Orgânica
Instituto de Química, Universidade Federal Fluminense
Niterói, RJ 24210–141 (Brazil)
[e] *Prof. L. C. Rodrigues Pereira da Silva*
Departamento de Fármacos e Medicamentos
Faculdade de Farmácia
Universidade Federal do Rio de Janeiro
Rio de Janeiro RJ 21941–599 (Brazil)
[+] *These authors contributed equally to this work.*

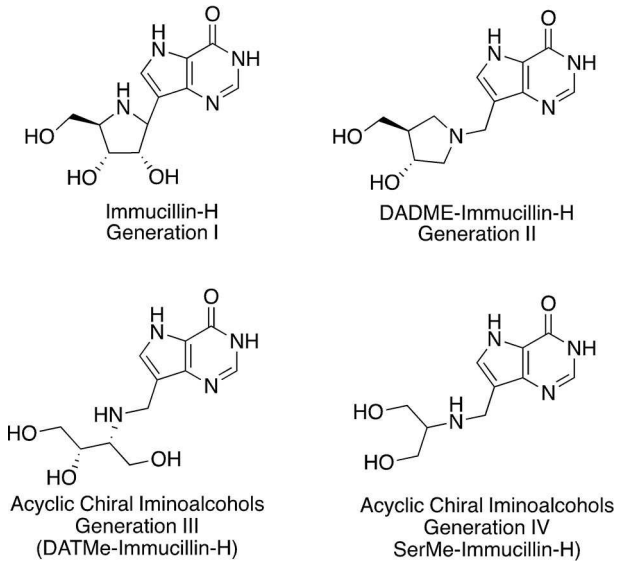

Figure 1. Four generations of PNP transition-state analogue inhibitors with dissociation constants in the picomolar range.

56 pM to *Hs*PNP.[6a,10b] The fully dissociative (S_N1) transition state of *Hs*PNP led to the second generation DADMe-Immucillins (4′-deaza-1′-aza-2′-deoxy-1′-(9-methylene)-Immucillins). These include a methylene bridge between the hydroxypyrrolidine mimic of the ribocation and the 9-deazapurine to mimic the fully dissociative transition state of *Hs*PNP. DADMe-Immucillin-H (clinically Ulodesine) binds tightly to *Hs*PNP, giving a dissociation constant of 8.5 pM.[9b,11] The third generation of Immucillins has the ribose ring replaced by an acyclic, chiral ribocation mimic (the acyclic chiral iminoalcohols). The tightest-binding inhibitor in this group is DATMe-Immucillin-H with an 8.6 pM dissociation constant for *Hs*PNP.[9b] The fourth generation transition state analogues for *Hs*PNP is represented by SerMe-Immucillin-H, an acyclic, achiral mimic of the ribocationic transition state with a 5.2 pM dissociation constant for *Hs*PNP.[9d] Despite their therapeutic potential, the clinical use of these PNP inhibitors is limited by their complex synthesis, high cost, and adverse side effects such as neutropenia, hypocalcemia, peripheral edema and orthostasis.[12] Thereby, the identification of new *Hs*PNP inhibitors holds promise for the treatment of proliferative T-cell disorders.

The rational design of enzyme inhibitors usually starts from a screening (through radiometric, spectrophotometric or chromatographic assays) of chemical libraries consisting of potential drug candidates. An activity assay, specific for the target enzyme, is developed to initially compare the inhibition percentage induced by different compounds, using a fixed concentration of enzyme, substrate and tested inhibitor. After this screening step, IC_{50} (inhibitor concentration that reduces the enzymatic activity to 50%) and K_i (enzyme–inhibitor dissociation constant) are determined for the most active molecules in order to quantify the inhibitor potency and the affinity for its target. The activity assay, in this case, is performed in presence of increasing amounts of inhibitors.[13]

Methods reported for PNP inhibition studies comprise radiometric and spectrophotometric assays[14] with specific drawbacks such as the use of radiolabeled compounds, or the need to couple a second enzyme (typically xanthine oxidase in the spectrophotometric assay) to achieve the required sensitivity. An innovative enzymatic method based on immobilized PNP in flow conditions has been reported for screening studies. However, the enzyme needs to be immobilized on the inner surface of silica capillaries and specific analytical skills are needed to run the experiments.[15] More recently, a 96-well enzymatic assay based on LC-ESI-MS/MS quantification for the identification of selective inhibitors against *Mycobacterium tuberculosis* PNP (*Mtb*PNP) was reported.[16] Nonetheless, the method requires the use of a sophisticated analytical platform amenable to high-throughput screening. HPLC-based enzymatic methods in combination with HPLC-UV detection are the simplest and most common approaches currently used to derive accurate and precise quantitative data.

In this paper, we report the discovery of a new *Hs*PNP inhibitor by integrated experimental and computational assays. For assessing the enzymatic activity of *Hs*PNP *in vitro*, we first developed a simple, inexpensive, non-radioactive, and reliable chromatographic assay based on hydrophilic interaction liquid chromatography (HILIC) and UV detection. Enzymatic reactions were carried out in batch and activity was determined by monitoring the phosphorolysis of inosine (Ino, substrate) to hypoxanthine (Hpx, product). Secondly, we reported the design and synthesis of a small library of both 6- and 8-substituted purine ribonucleosides for screening as potential *Hs*PNP inhibitors. The assay, based on LC-UV using HILIC as elution mode, was used for characterizing the kinetics of *Hs*PNP, screening the library of purine nucleoside analogues as potential enzyme inhibitors, and quantitatively assessing the inhibitory activity of the most active candidate, 8-aminoinosine (**4**). Quantum chemical approaches were applied to determine the most favorable tautomeric form of purine nucleoside analogue **4** in the gas phase and aqueous solution. Moreover, to provide insights into inhibitor binding at molecular level and facilitate the design of more potent ligands, we also performed docking studies of **4** into *Hs*PNP catalytic site. Finally, **4** was tested under different conditions in CCRF-CEM lymphocytes cell cultures which highly express *Hs*PNP. Altogether, this paper describes a novel pipeline for screening *Hs*PNP inhibitors *in vitro*, as well as the discovery of a new *Hs*PNP lead inhibitor.

Results and Discussion

Design and synthesis of nucleosides 2–10

To identify new selective inhibitors of *Hs*PNP, we designed and synthesized a small library of both 6- and 8-substituted purine ribonucleosides (Figure 2) based on the evidence that some related analogues had been reported to inhibit *Hs*PNP (e.g., 8-aminoguanosine, $K_i = 17\ \mu M$).[17] Moreover, the inhibition data recently collected for some 8-halo-, 8-amino-, 8-*O*-alkyl-substituted purine ribonucleosides[16] prompted us to select new

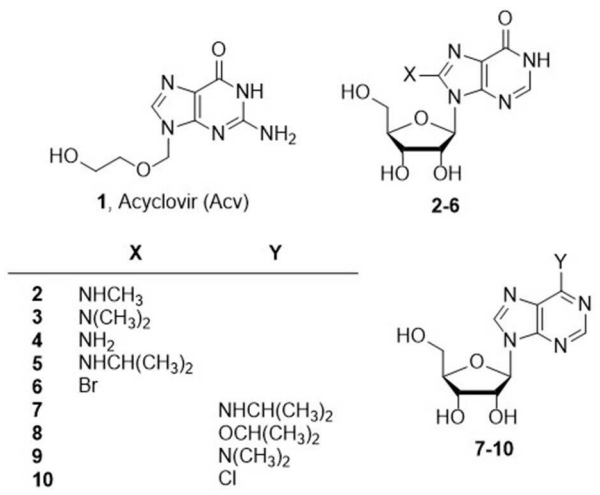

Figure 2. Structures of the nucleoside analogues tested as potential inhibitors.

congeners. Specifically, the new set of nucleosides includes four 8-aminoinosine derivatives bearing a differently sterically hindered substituent [8-methylaminoinosine (**2**), 8-*N,N*-dimethylaminoinosine (**3**), 8-aminoinosine (**4**), 8-*i*-propylaminoinosine (**5**)], and 8-bromoinosine (**6**). From the 6-substituted series, 6-*i*-propylaminopurine-9-riboside (**7**) and its isostere counterpart 6-*i*-propoxypurine-9-riboside (**8**), 6-dimethylaminopurine-9-riboside (**9**), and 6-chloropurine-9-riboside (**10**) were chosen. Compounds **2** and **3** were previously found to inhibit *Hs*PNP[6] and were thus used as reference controls together with acyclovir (Acv, **1**).

The 6-substituted purine ribonucleosides (**7**–**10**) were prepared as previously reported.[18]

The synthesis of 8-substituted inosines (**2**–**5**) was achieved through a similar approach, that is, by halogenation of the purine ring and subsequent treatment with the appropriate nucleophile. Specifically, to prepare compound **5**, 2′,3′,5′-tri-*O*-acetyl-8-bromoinosine (**11**)[18a] was treated with isopropylamine in 1,4-dioxane at 80 °C in 25% yield (Scheme 1). Because of the slow reactivity of position 8 in purines, which is generally less prone to nucleophilic attack than 2- and 6-positions, long reaction times as well as high reagent concentrations were required. On the other hand, 8-aminoinosine (**4**) was obtained from the corresponding benzyl derivative (**12**), prepared by treatment of **11** with benzylamine, by prolonged hydrogenolysis with $HCOONH_4$ in MeOH in the presence of Pd–C (10 mol%) as catalyst (Scheme 1). The low yield of the synthesis of **5** (25%) in comparison with that of **12** (83%) might be attributed to the steric hindrance and high volatility of isopropylamine.

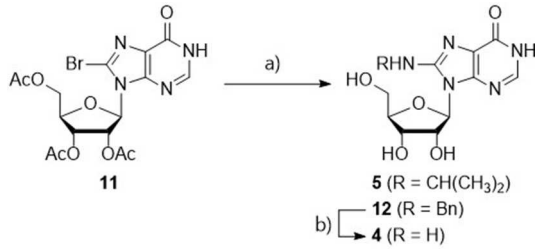

Scheme 1. Synthesis of compounds **4** and **5**. a) $iPrNH_2$ or $BnNH_2$, 1,4-dioxane, 80 °C (25% for **5** and 83% for **12**); b) $HCOONH_4$, Pd/C (10 mol%), MeOH, reflux (96%).

LC-UV method development

A method based on LC-UV using HILIC as elution mode was developed to monitor the phosphorolysis of Ino to Hpx and consequently *Hs*PNP activity under different conditions. The chromatographic conditions that allowed us to properly separate and quantify Ino, Hpx and their internal standards [Acv and 2′-deoxyadenosine (dAdo), respectively] required the use of a carbamoyl TSKgel Amide-80 column and a mobile phase composed of acetonitrile (ACN)/15 mM ammonium formate buffer (92:8, *v/v*, pH 7.0), as described in the Experimental Section. Figure 3 shows the chromatogram obtained by applying the method described. The linearity of the method was established for both the substrate (Ino) and product (Hpx) in the concentration range 0.5–50 μM. Calibration curves of $y = 0.1192x + 0.0601$ ($R^2 = 0.9987$) and $y = 0.1225x + 0.0379$ ($R^2 = 0.9984$) were obtained for Ino/Acv and Hpx/dAdo, respectively.

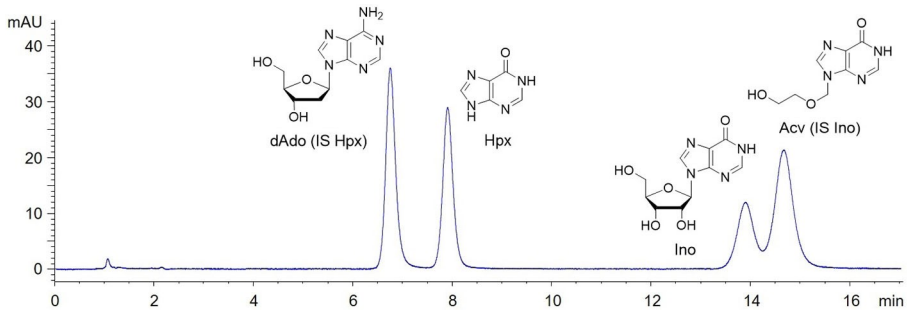

Figure 3. Representative chromatogram of Ino, Hpx and their internal standards.

Enzymatic activity assay

Kinetic and inhibition enzymatic assays were performed following the procedures reported in the Experimental Section. At the endpoint of the enzymatic reactions (5 min), the enzyme was inactivated by diluting the reaction mixture in acetonitrile containing internal standards. Before the quantification of the produced Hpx by LC-UV, the denatured enzyme was separated from the supernatant through centrifugation.

Kinetic studies

*Hs*PNP was incubated with increasing amounts of Ino (0.01–1 mM, three replicates for each concentration) to measure the enzyme activity. Since the reaction catalyzed by PNPs requires the presence of inorganic phosphate (P_i) as a second substrate, the assay was performed in 10 mM ammonium phosphate buffer, pH 7.5, used as a source of P_i in saturating concentration. Kinetic parameters are reported in Table 1, while Michaelis–Menten kinetics are shown in Figure 4. The obtained values are consistent with and of the same order of magnitude as those reported by Cattaneo et al.[16]

Inhibition studies

After demonstrating the reliability of the enzymatic assay in the determination of *Hs*PNP activity, the synthesized 6- and 8-substituted purine ribonucleosides (Figure 2) were tested as inhibitors. The inhibition induced by the different candidates was initially determined by performing a screening assay. Thus, the enzymatic activity assay was carried out at fixed concentrations of the *Hs*PNP substrate (close to the K_M for Ino, saturating for P_i) and of the inhibitor candidates (0.5 mM). The enzyme activity was calculated in presence and in absence of each candidate and inhibition percentages (expressed as enzyme residual activity) were compared.

Most of the assayed nucleoside analogues showed a *Hs*PNP inhibition below 30% (Figure 5). Compound **4** was the only exception, and it was thus selected for further studies (29.26 ± 1.75% *Hs*PNP residual activity) aimed at assessing inhibition potency and enzyme affinity through K_i and IC_{50} determination.

K_i measures the enzyme-inhibitor dissociation constant, while IC_{50} expresses the inhibitor concentration required to obtain a 50% reduction in enzyme activity. Both K_i and IC_{50} quantify inhibitor potency, but usually K_i is preferred because, unlike IC_{50}, it is independent from substrate identity and concentration.[13] For K_i and IC_{50} determination, the activity assay was performed under the same conditions used for the screening assays, but with increasing inhibitor concentrations (0.01–1 mM, three replicates). Residual activity of *Hs*PNP was calculated by comparing the results obtained in presence and in absence of each nucleoside. The two inhibition parameters were calculated by fitting the curve of inhibitor concentrations ($\log M$) versus residual activities [%] through Prism® software (see the Experimental Section).

Data reported in Table 2 confirmed the information derived from the screening assay and provided a quantitative assessment of the inhibitory activity of **4**, being K_i and IC_{50} in the micromolar range.

Structural basis of *Hs*PNP inhibition by 8-aminoinosine (4)

In an effort to elucidate the possible binding mode of compound **4** within *Hs*PNP active site, we carried out docking

Table 1. *Hs*PNP kinetic parameters (K_m, V_{max} and k_{cat}). Values were calculated using Ino as the substrate.

Enzyme	K_M [mM]	V_{max} [μmol/min]	k_{cat} [s^{-1}]
*Hs*PNP	0.1267 ± 0.0213	0.0078 ± 0.0004	52.52 ± 3.00

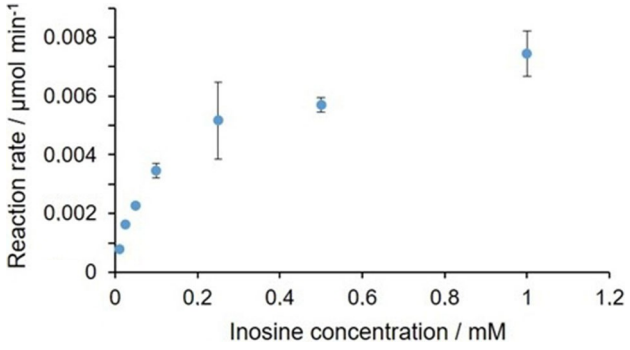

Figure 4. Kinetic profile of *Hs*PNP. The enzyme was incubated with increasing concentrations of Ino. Each point is the mean of three replicates, with error bars indicating ± standard deviation.

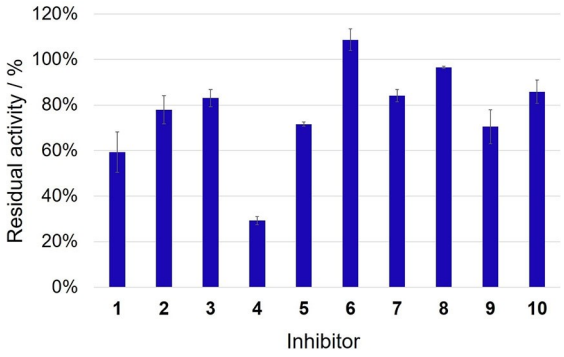

Figure 5. Residual activity of *Hs*PNP upon incubation with 0.5 mM of each nucleoside analogue (**1**–**10**). Results derive from the mean of three independent determinations, with standard deviation indicated by error bars. A residual activity of 100% corresponds to the produced Hpx in absence of the potential inhibitor.

Table 2. Inhibition results of 8-aminoinosine (**4**) towards *Hs*PNP.

Inhibitor	Enzyme	K_i [mM]	$\log K_i$ $\log M$	IC_{50} [mM]	$\log IC_{50}$ $\log M$
4	*Hs*PNP	0.0481	−4.32 ± 0.0539	0.0860	−4.06 ± 0.0539

experiments using the crystal structure of *Hs*PNP in complex with the transition-state analogue l-DADMe-ImmH (PDB ID: 3BGS[19]).

Purine derivatives can exist in different keto-enol and amino-imino tautomeric forms. The potential structures which may be adopted by **4** are presented in Figure 6. Thus, before docking into the PNP active site, we carried out separate quantum chemical calculations on the possible tautomeric forms of **4** and their relative stability (**A**–**F** in Figure 6). The ground-state molecular geometries of the tautomers were optimized at the MP2/6-311G** level of theory.[20]

Geometries of the selected tautomers were also optimized in water solution using the integral-equation-formalism polarizable continuum model (IEF-PCM). The resulting energies were combined with the thermochemical corrections computed using the same approach to yield the Gibbs free energies and the Boltzmann population ratios (BPRs) at 298.15 K. The results are summarized in Table 3. Both the MP2 and IEF-PCM methods predicted that the most stable and dominant tautomer of **4** corresponds to the keto form **A** with BPRs at 298 K of 81.76 and 99.64%, respectively. The second stable structure was the tautomer **B**, which is characterized by the presence of an enol group connected to the C6 carbon atom. The Gibbs free energy difference is less than 1 kcal/mol in gas phase and more than 3 kcal/mol in solution. However, the enol tautomer **B** was predicted to be much less abundant with BPRs at standard temperature of 18.24% in gas phase and 0.36% in solution. This agrees with experimental evidence, which clearly indicates that Ino exists as the N1H keto species in gas phase[21] and aqueous solutions[22] and this is also the structure determined crystallographically.[23]

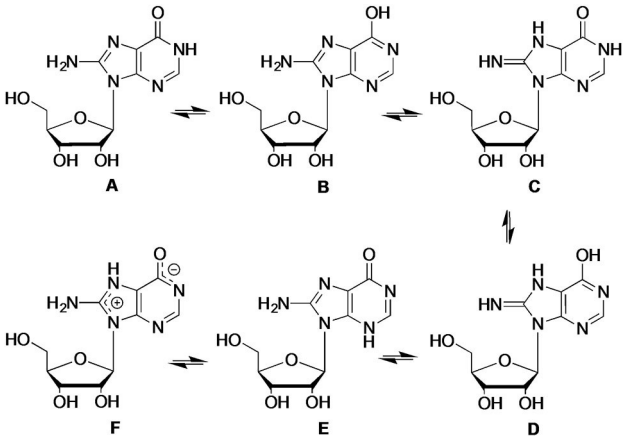

Figure 6. Structures of the six possible tautomeric forms of 8-aminoinosine (**4**, **A**–**F**).

Docking simulations into the *Hs*PNP active site showed that the keto form of compound **4** adopted a binding mode very similar to that previously reported for l-DADMe-ImmH[19] (Figure 7B) in terms of orientation within the active site, interactions with the enzyme, as well as docking score (CHEMscore fitness = 36.1, CHEMscore $\Delta G_{bind} = -39.9$ kJ/mol). As depicted in Figure 7A, the ligand forms three H-bonds between the purine O6, N7H and 8-NH_2 groups and N243 side chain. A further H-bond between the 8-NH_2 group and T242 residue within the catalytic site is also observed, thus contributing to the complex stabilization. The purine N1 and O6 (via a water molecule) atoms are also in H-bond distance to E201. The 5′–OH group makes a H-bond to the imidazole ring of H257. The 3′–OH group establishes a H-bond with the OH group of Y88. Finally, the 2′–OH group interacts with the amide backbone of M219 and a structurally observed water molecule.

In vitro effect of 8-aminoinosine (4) on CCRF-CEM

The effects of **4** on T-cell leukemia cell line CCRF-CEM were evaluated by treating cell cultures with increasing concentrations of **4** for 96 hours in the presence or absence of dGuo (0 or 10 μM), which mimics the extracellular accumulation of this metabolite in *Hs*PNP deficiency.[24] Figure 8 shows the CCRF-CEM viability after treatment with **4**. The significant differences between cell viabilities in the presence or absence of dGuo evidence the inhibitory activity of compound **4**. With *Hs*PNP inhibition, intracellular dGuo is metabolized into dGTP by cellular kinases, which alters the balance within the deoxynucleotide pool, resulting T-cell death via a characteristic mechanism of apoptosis induction.[25] Nucleoside **4** was able to reduce CCRF-CEM viability in the absence of dGuo (0 μM) only at 250 μM, showing its intrinsic cytotoxic effect only at high concentrations. From 10 to 100 μM, nucleoside **4** significantly reduced cell viability in the presence of 10 μM dGuo, demonstrating that the CCRF-CEM cell viability was decreased exclusively by PNP inhibition effect in this range. CCRF-CEM T-lymphocytes present low dGMP catabolism and high rates of dGuo phosphorylation, leading to even more pronounced toxic effects during *Hs*PNP inhibition.[6a]

Table 3. Relative values of the total energies (ΔE [kcal/mol]) and the Gibbs (ΔG [kcal/mol]) free energies of the different tautomers of **4** calculated at the MP2/6-311G** level of theory in the gas phase and in the solution by using the IEF-PCM model along with the results of the Boltzmann population weighted analysis (BPR, %).

Molecule	Tautomer	Gas phase MP2			Solution IEF-PCM		
		ΔE	ΔG	BPR	ΔE	ΔG	BPR
8-aminoinosine (**4**)	**A**	0.0	0.0	81.76	0.0	0.0	99.64
	B	0.78	0.89	18.24	3.96	3.33	0.36
	C	15.01	13.82	0	15.41	13.48	0
	D	14.31	13.36	0	17.78	15.12	0
	E	22.98	21.69	0	15.26	14.25	0
	F	23.93	23.14	0	15.45	15.18	0

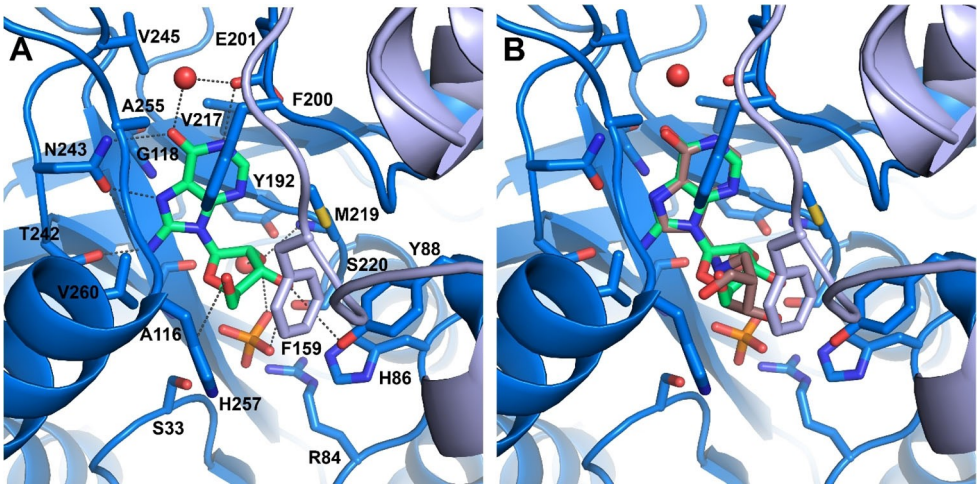

Figure 7. *In silico* docking of compound **4** into *Hs*PNP active site. A) Binding mode of **4** (green sticks) into the *Hs*PNP active site located near the interface of two subunits (blue and lilac ribbons for *Hs*PNP) within the trimer. Only amino acids located within 4 Å of the bound ligand are displayed and labeled. H-bonds discussed in the text are depicted as dashed gray lines. Phosphate is shown as orange sticks; structural water molecules are displayed as red spheres. B) Cα superposition of the complex of *Hs*PNP with 8-aminoinosine (**4**) and I-DADMe-ImmH (orange sticks), a 2 pM transition-state analogue inhibitor.

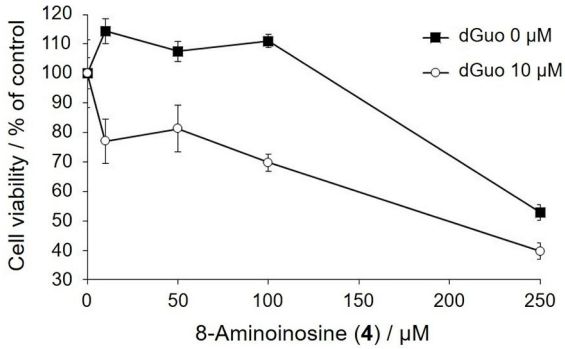

Figure 8. Cytotoxic effects of 8-aminoinosine (**4**) on the T-cell leukemia cell line CCRF-CEM in the presence/absence of dGuo. Cell-growing conditions and the method of measurement are described in the Experimental Section. Control values for dGuo absence were obtained by cell incubation without dGuo and **4**. Control values in the presence of dGuo were obtained by cell incubation with 10 μM dGuo and 0 μM **4**. Each data point represents a mean across 4 experiments.

Conclusion

Driven by the evidence that *Hs*PNP plays a significant role in peripheral T-cell lymphoma, we designed and synthesized a small library of 6- and 8-substituted purine ribonucleosides as potential enzyme inhibitors (Figure 2). Compounds were designed taking into account previous reports on the inhibition activity of nucleoside analogues against *Hs*PNP.[16,17] Starting from the conditions described in a previous work from some of the Authors,[16] we developed an enzymatic assay by LC-UV using HILIC as elution mode. The assay is based on the in batch phosphorolysis of Ino to Hpx and quantification of the reaction conversion in the presence of nucleoside-based inhibitor candidates. This method is characterized by sensitivity and specificity, it does not need the use of radiolabeled compounds and relies on a user-friendly instrumentation commonly available in any drug discovery lab. Moreover, the method is MS-compatible in view of a future application in screening studies of broader libraries of potential inhibitors.

The linearity of the LC-UV method was assessed by using the internal standard approach and no matrix effect due to the presence of denatured enzyme was observed, thus confirming that the centrifugation step after the enzymatic reaction was sufficient to separate PNP from Ino, Hpx and their internal standards. In addition, since solubilization of nucleosides required the use of dimethylsulfoxide (DMSO), the enzymatic assay was performed both in presence and in absence of DMSO and no significant differences on the enzymatic activity were observed.

Before starting with the investigation of potential enzyme inhibitors, it is necessary to characterize the target enzyme by defining its activity in absence of inhibitor. Enzymatic activity assays quantify the product formation or the substrate consumption over time to define reaction rate. The kinetic properties of most enzymes can be described by the Michaelis–Menten equation. The maximum reaction rate V_{max} and K_M, which is the substrate concentration that allows half of the V_{max} to be reached, were determined. Another important kinetic parameter to assess enzyme activity is the turnover number k_{cat}, which expresses the number of substrate molecules converted into product per catalytic site per unit of time.

The enzymatic assay was therefore applied to the kinetic characterization of *Hs*PNP by the definition of V_{max}, K_M and k_{cat}; all parameters were found to be consistent with the data previously reported by Cattaneo et al.[16] For the preliminary screening step, only one fixed concentration of substrates (Ino and P_i), inhibitors and enzyme was tested. The concentration of Ino was set close to the K_M value, reaction buffer was used as a source of P_i in saturating concentration, the inhibitors were tested at the highest concentration dictated by the solubility of the compounds under the assay conditions, and the same

amount of enzyme for the kinetic studies was added. *Hs*PNP residual activity was calculated by comparing the produced Hpx in presence and in absence of each compound. As shown in Figure 5, in addition to the control inhibitor Acv, compound **4** was found to considerably inhibit *Hs*PNP, being the residual activity of *Hs*PNP 29.26 ± 1.75 %. The inhibition potency of nucleoside **4** was assessed by performing the enzymatic assay in presence of increasing amounts of inhibitor, while all the other conditions were the same as for the screening. K_i and IC_{50} values confirmed the significant inhibitory activity of **4**.

Quantum chemical calculations on the possible tautomeric forms (**A**–**F** in Figure 6) of **4** clearly demonstrated that this compound exists predominantly as keto form **A** both in gas phase and aqueous solution, which is in agreement with previous theoretical and experimental findings.[21–23,26] To elucidate the possible binding mode of compounds **4** within *Hs*PNP active site and to shed light onto the structural determinants underlying its inhibitor activity, a docking study was also performed. In addition, compound **4** significantly reduced cell viability of T cell leukemia cell line CCRF-CEM in the presence of 10 μM dGuo. In contrast, in the absence of dGuo, the reduction of cell viability was negligible, thus suggesting that this effect is associated to PNP inhibition, which results in intracellular dGuo metabolization into dGTP, an inhibitor of DNA synthesis and cellular proliferation.

In conclusion, we developed a straightforward assay for evaluating the activity of *Hs*PNP and screening *Hs*PNP inhibitors.

Experimental Section

Reagents and chemicals

The *Hs*PNP recombinant enzyme was kindly provided by Prof. Diógenes Santiago Santos (PUC-RS, in memoriam). *Hs*PNP activity was 0.57 IU/mg (stock solution: 0.4 mg/mL).[16] Water was obtained from a Milli-Q® Integral system (Merck). Acetonitrile HPLC grade, ammonium phosphate monobasic (≥ 99 %) and ammonium formate (≥ 99 %) were purchased from Sigma–Aldrich, while dimethylsulfoxide was from Carlo Erba Reagents (Cornaredo, Italy). Hypoxanthine (Hpx) was from Alfa Aesar. Inosine (Ino), acyclovir (Acv, **1**) and 2′-deoxyadenosine (dAdo) were purchased from Sigma–Aldrich. 8-Methylaminoinosine (**2**), 8-*N*,*N*-dimethylaminoinosine (**3**), 8-bromoinosine (**6**), 6-*i*-propylaminopurine-9-riboside (**7**), 6-*i*-propoxypurine-9-riboside (**8**), 6-dimethylaminopurine-9-riboside (**9**) and 6-chloropurine-9-riboside (**10**) were synthesized as previously reported.[16,18]

8-Aminoinosine (4): 8-Benzylamino inosine[27] (**12**, 60 mg, 0.16 mmol) and 10 % Pd-C (90 mg) were suspended in MeOH (2.50 mL) under inert atmosphere and treated with $HCOONH_4$ (202 mg, 3.20 mmol); the resulting mixture was refluxed and monitored by TLC (CH_2Cl_2/MeOH, 4:1). Further portions of $HCOONH_4$ were progressively added over 5 days (202 mg, 3.20 mmol after 24 h, 404 mg, 6.41 mmol after 96 h and 101 mg, 1.60 mmol after 120 h). The suspension was then filtered on celite and evaporated under reduced pressure to get the title compound as a pale yellow powder (43 mg, 0.15 mmol, 96 % yield). R_f: 0.10 (CH_2Cl_2-MeOH, 4:1). ^{1}H NMR ([D_6]DMSO, 400 MHz): δ = 3.63 (br s, 2H, $H^{5'a}$, $H^{5'b}$), 3.94 (br q, J = 2.3 Hz, 1H, $H^{4'}$), 4.12 (dd, J = 5.4, 2.0 Hz, 1H, $H^{3'}$), 4.59 (t, J = 6.4 Hz, 1H, $H^{2'}$), 5.16 (br s, 1H, $OH^{3'}$), 5.30 (br s, 1H, $OH^{2'}$), 5.56 (br s, 1H, $OH^{5'}$), 5.85 (d, J = 7.3 Hz, 1H, $H^{1'}$), 6.50 (br s, 2H, N^8H_2), 7.79 (s, 1H, H^2), 12.04 ppm (br s, 1H, N^1H); ^{13}C NMR ([D_6]DMSO, 100 MHz): δ = 61.8 ($C^{5'}$), 71.0 ($C^{2'}$), 71.2 ($C^{3'}$), 86.2 ($C^{4'}$), 87.2 ($C^{1'}$), 120.9 (C^5), 143.0 (C^2), 147.5 (C^4), 151.1 (C^8), 155.4 ppm (C^6); MS (ESI$^+$): *m/z* 284.0 $[M+H]^+$, 306.1 $[M+Na]^+$, 567.0 $[2M+H]^+$, 589.0 $[2M+Na]^+$.

8-(*i*-Propylamino)inosine (5): To a solution of 2′,3′,5′-*O*-triacetyl-8-bromoinosine[18a] (**11**, 189 mg, 0.40 mmol) in dry 1,4-dioxane (0.9 mL) was added a large excess of isopropylamine (3.22 mL, 37.4 mmol) under a N_2 atmosphere. The mixture was stirred at 80 °C and monitored by TLC (CH_2Cl_2-MeOH, 4:1) until complete consumption of the starting material. The solvent was removed under reduced pressure and the residue was purified by semipreparative HPLC (see below for chromatographic conditions) to give the title compound as a white powder (32 mg, 25 % yield). R_f: 0.32 (CH_2Cl_2/MeOH, 4:1). ^{1}H NMR ([D_6]DMSO, 400 MHz): δ = 1.18 (d, J = 3.4 Hz, 3H, $CH(CH_3)_2$), 1.20 (d, J = 3.5 Hz, 3H, $CH(CH_3)_2$), 3.61-3.71 (m, 2H, $H^{5'a}$, $H^{5'b}$), 3.95 (br q, J = 2.1 Hz, 1H, $H^{4'}$), 3.97-4.07 (m, 1H, NHC*H*), 4.12 (dd, J = 5.5, 2.0 Hz, 1H, $H^{3'}$), 4.54 (dd, J = 7.1, 5.8 Hz, 1H, $H^{2'}$), 4.96-5.48 (m, 2H, $OH^{2'}$, $OH^{3'}$), 5.63 (br s, 1H, $OH^{5'}$), 5.89 (d, J = 7.4 Hz, 1H, $H^{1'}$), 6.59 (d, J = 7.6 Hz, 1H, N^8H), 7.81 (s, 1H, H^2), 12.01 ppm (br s, 1H, N^1H); ^{13}C NMR ([D_6]DMSO, 100 MHz): δ = 22.8, 23.1 ($CH(CH_3)_2$), 44.4 (NHCH), 61.8 ($C^{5'}$), 70.9 ($C^{2'}$), 71.2 ($C^{3'}$), 86.0 ($C^{4'}$), 87.0 ($C^{1'}$), 122.2 (C^5), 142.5 (C^2), 147.9 (C^4), 150.5 (C^8), 155.9 ppm (C^6); MS (ESI$^+$): *m/z* 326.0 $[M+H]^+$, 348.2 $[M+Na]^+$, 673.1 $[2M+Na]^+$.

Instrumentation and chromatographic conditions

Semipreparative HPLC was performed using an ÄKTA Basic100 instrument (Amersham Pharmacia Biotech, Little Chalfont, UK) equipped with a UV/Vis detector (Pharmacia, Uppsala, Sweden); chromatographic conditions were as follows: column, Jupiter® 10 μm Proteo 90 A (250 × 10.0 mm, Phenomenex); flow rate, 5 mL/min; detector, λ = 260 and 250 nm; mobile phase MeOH/H_2O, isocratic elution at 3 % MeOH for 2 min, then gradient elution from 3 to 100 % MeOH over 30 min. ^{1}H and ^{13}C NMR spectra were recorded at 400.13 and 100.61 MHz, respectively, on a Bruker AVANCE 400 spectrometer equipped with the XWIN-NMR software package (Bruker) at 300 K. ^{1}H and ^{13}C chemical shifts (δ) are given in parts per million and were referenced to the solvent signals (δ_H = 2.50 and δ_C = 39.50 ppm for [D_6]DMSO). ^{13}C NMR signal multiplicities were based on APT (attached proton test) spectra. Electrospray ionization mass spectra (ESI-MS) were acquired on a ThermoFinnigan LCQ Advantage spectrometer.

Analytical HPLC was performed on an Agilent HPLC series 1100 system, equipped with mobile-phase online degasser, quaternary pump, autosampler, column thermostated compartment and diode array detector. For data acquisition and analysis, the HP ChemStation for LC software version Rev. A.06.03 [509] was used. A TSKgel Amide-80 (3 μm, 80 Å, 2 × 150 mm) column from Tosoh Bioscience (Montgomeryville, PA, USA) was employed. The mobile phase was composed of a mixture of ACN and 15 mM ammonium formate 92:8 (*v*/*v*), pH 7.0. Chromatographic conditions consisted of an isocratic elution for 17 min, a temperature of 25 °C, an injection volume of 10 μL and a constant flow rate of 300 μL/min. In all experiments, compounds were detected at 254 nm. The linearity of the method was assessed for Ino and Hpx in the concentration range 0.5–50 μM. Eight concentration levels were considered, and three independent determinations were performed for each point. A fixed amount (5 μM) of the internal standards dAdo and Acv was added to each sample. Calibration curves were obtained by the least squares method plotting Hpx/dAdo and Ino/Acv peak area ratios (*y*-axis) against Hpx and Ino concentrations (*x*-axis), respectively.

Sample preparation: For the calibration curve determination, stock solutions of 10 mM Ino (in water), Hpx, dAdo and Acv (in DMSO) were prepared. Working solutions (0.025, 0.25, and 1 mM for Ino and Hpx, 0.25 mM for dAdo and Acv) were obtained by dilution of the stock solutions in water. The working solutions of compounds and internal standards were then combined and made up to a 500 μL final volume with ACN in order to reach the required concentrations.

For the enzymatic assay, 10 mM Ino (in water) and inhibitor (in DMSO) stock solutions were diluted to different concentrations with 10 mM ammonium phosphate, pH 7.5 to reach a volume of 480 μL. The addition of 20 μL of enzyme solutions, prepared by diluting 1:100 the *Hs*PNP stock solution (see reagents and chemicals), allowed to obtain the final volume (500 μL) for the reaction.

Enzymatic activity assay

The procedure followed for the enzymatic assays was adapted to the available laboratory equipment starting from the protocol described by Cattaneo and colleagues.[16] Briefly, microcentrifuge tubes containing 480 μL solutions of Ino and phosphate buffer for the kinetic assay or Ino, phosphate buffer and inhibitor for the inhibition assay, were conditioned for 5 min at 37 °C under continuous stirring. Then, 20 μL enzyme solution (see sample preparation) were added to each tube (0.08 μg *Hs*PNP/microcentrifuge tube). The reaction was run for 5 min at 37 °C under continuous stirring and subsequently stopped by pipetting 25 μL of the reaction mixture in a new microcentrifuge tube containing 475 μL ACN and the internal standards (1.05 μM of dAdo and Acv). The obtained solutions were mixed by pipetting 150 μL up and down for three times and the inactivated enzyme was removed by centrifugation (2655×g for 10 min). Finally, the supernatant was analyzed by LC-UV using HILIC as elution mode.

Kinetic studies: In the Michaelis–Menten equation:

$$v = \frac{V_{max}\,[S]}{K_M + [S]}$$

v is the reaction rate, V_{max} is the maximum reaction rate, [S] represents the concentration of the substrate and K_M, or Michaelis–Menten constant, is the substrate concentration that allows to reach half of the V_{max}. The turnover number k_{cat} expresses the number of substrate molecules converted into product per catalytic site per unit of time and is given by the ratio between enzyme concentration and V_{max}.

Ino kinetic constants were defined by performing the enzymatic assay in presence of increasing Ino concentrations (seven concentrations in the range 0.01–1 mM, mean of three replicates) and a fixed amount of P_i (10 mM ammonium phosphate, pH 7.5). To calculate reaction rates of *Hs*PNP, μmol of produced Hpx were derived taking into account the Hpx/dAdo calibration line and were divided by the reaction time (5 min). The Michaelis–Menten trend was obtained by plotting the rate of the enzymatic reaction, expressed as μmol of produced Hpx/min, against the substrate (Ino) concentration [mM]. The kinetic parameters V_{max} (maximal reaction rate [μmol/min]), K_M (Michaelis–Menten constant [mM]) and k_{cat} (turnover number [s^{-1}]) were calculated by Prism® software (GraphPad Software) using a nonlinear regression curve fitting. To define V_{max} and K_M, the Michaelis–Menten model $Y = V_{max} \times X/(K_M + X)$ was chosen. The enzyme kinetics equation $Y = E_t \times K_{cat} \times X/(K_M + X)$ was used to determine k_{cat}. The term E_t represents the concentration of enzyme catalytic sites and it was calculated considering that *Hs*PNP (MW = 96354 Da) is homotrimeric.

Inhibition studies: The enzymatic assay was applied to the screening of ten nucleoside analogues (acyclovir (**1**), 8-methylaminoinosine (**2**), 8-*N,N*-dimethylaminoinosine (**3**), 8-aminoinosine (**4**), 8-*i*-propylaminoinosine (**5**), 8-bromoinosine (**6**), 6-*i*-propylaminopurine-9-riboside (**7**), 6-*i*-propoxypurine-9-riboside (**8**), 6-dimethylaminopurine-9-riboside (**9**) and 6-chloropurine-9-riboside (**10**)) as potential PNP inhibitors. The assay was carried out by using a high inhibitor concentration (0.5 mM) and fixed concentrations of Ino (close to the K_M value: 0.1 mM) and P_i (10 mM ammonium phosphate, pH 7.5). *Hs*PNP residual activity [%] was calculated by comparing the produced Hpx in presence of each inhibitor to the reaction carried out under the same conditions, but in absence of inhibitor (100% residual activity). Each resulting percentage is the mean of three replicates. Inhibition constants (K_i) were assessed in the same conditions of the screening assay, except for the amount of inhibitors. Five concentrations of each inhibitor (0.01–1 mM, three replicates) were incubated with *Hs*PNP and reactions without inhibitor were carried out in parallel. Residual activity [%] of *Hs*PNP was calculated considering the Hpx/dAdo calibration line, the dilution factor and the assay volume (500 μL), and was plotted against the inhibitor concentration [μM] in a logarithmic scale. K_i and IC_{50} (inhibitor concentration that gives 50% of the maximal response) parameters were calculated by Prism® software (GraphPad Software, San Diego, CA, USA) according to the One site – Fit K_i (1) and One site – Fit LogIC_{50} (2) equations, respectively:

$$\log IC_{50} = \log(10 \log K_i \cdot (1 + [Ino]/InoK_M)) \quad (1)$$

$$Y = (top - bottom)/(1 + 10\,(X - \log IC_{50})) + bottom \quad (2)$$

where K_i and IC_{50} are expressed in M, [Ino] is the constant concentration of substrate [M], InoK_M is the Michaelis–Menten constant of the substrate [M], top and bottom represent the plateaus reached on the *y*-axis [%].

Computational chemistry

Molecular modeling and graphics manipulations were performed using Maestro 11.0 (Schrödinger, LLC, New York, NY, 2017) and UCSF-Chimera 1.8.1 (http://www.cgl.ucsf.edu/chimera) software packages running on a E4 Computer Engineering E1080 workstation provided with an Intel Xeon processor. GOLD Suite 5.5 docking package (CCDC Software Limited: Cambridge, UK)[28] was used for all docking calculations. All quantum chemical calculations were performed with the Gamess-US program.[29] Figures were generated by using PyMOL 2.0 (Schrödinger, 2017).

Quantum chemical calculations: The initial tautomeric structure of **4** was built with the Avogadro program[30] and the geometry optimized by using B3LYP method with 6–311G** basis set. The level of theory was then increased using the second-order Møller-Plesset perturbation theory (MP2)[20] with the triple-ζ quality Gaussian-type basis sets augmented with polarization functions (def2-TZVP).[31] This kind of calculations allowed us to obtain more reliable electrons wave functions and stationary nuclei coordinates. To mimic aqueous solutions, the IEF-PCM model[32] was applied. The IEF-PCM model defines the cavity within the solvent as the union of a series of interlocking atom spheres and is considered more effective when a higher accuracy in the results is required for the solvent-solute interactions.[33] To ensure that the optimized geometries represented the local minima and that there were only positive eigenvalues, vibrational frequencies and approximate description of each normal modes were also carried out using MP2/

6-311G** in both gas and liquid phase. The vibrational calculations were carried out within the harmonic approximation. BPRs of the tautomer in vacuum and water at room temperature ($T = 298.15$ K) were calculated using the Boltzmann distribution formula:

$$n_i = \frac{e^{\frac{-(G_i - G_0)}{RT}}}{\sum_n e^{\frac{-(G_n - G_0)}{RT}}} \times 100$$

where n_i is the population [%] of the ith tautomer, G_i the Gibbs energy of the ith tautomer and G_0 the Gibbs energy of the most stable tautomer.

Protein and ligand preparation: The crystal structure of *Hs*PNP in complex with the transition-state analogue l-DADMe-ImmH (PDB ID: 3BGS),[19] recovered from Brookhaven Protein Database,[34] was employed for the automated docking experiment. The protein was processed through the Protein Preparation Wizard in Maestro. Apart from two structural water molecules and a phosphate anion that are critical in creating catalytic activity, all crystallographic water molecules and other chemical components were deleted. The right bond orders as well as charges and atom types were assigned, and the hydrogen atoms were added. Arginine and lysine side chains were considered as cationic at the guanidine and ammonium groups, and the aspartic and glutamic residues were considered as anionic at the carboxylate groups. H257 in *Hs*PNP was modeled in the neutral form with the proton at NE leaving ND1 to interact with 5′-OH of the ribose ring.[35] Moreover, an exhaustive sampling of the orientations of groups, whose H-bonding network needs to be optimized, was performed. Finally, the protein structure was refined with a restrained minimization with the OPLS2005 force field[36] by imposing a 0.3 Å rmsd limit as the constraint.

The core structure of compound **4** was built using the Molecular Builder module in Maestro. Atom N7 of the ligand was protonated because transition state analysis[9a] has established its protonation to N7H before reaching the transition state. The ligand was then preprocessed with LigPrep 3.3 (Schrödinger, 2017) and optimized by Macromodel 10.7 (Schrödinger, 2017), using the MMFFs force field with the steepest descent (1000 steps) followed by truncated Newton conjugate gradient (500 steps) methods. Partial atomic charges were computed using the OPLS-AA force field.

Docking simulations: Docking of **4** to *Hs*PNP was performed with the GOLD software,[28] which uses a genetic algorithm for determining the docking modes of ligands and proteins. The coordinates of the cocrystallized transition-state analogue l-DADMe-ImmH were chosen as active-site origin. The active-site radius was set equal to 6 Å. Two explicit water molecules were allowed to toggle on or off during the individual docking runs (i.e., these waters were not automatically present in the binding site, but were included if their presence strengthened the interaction of the ligand with the receptor, as determined by the scoring function).[37] Each GA run used the default parameters of 100000 genetic operations on an initial population of 100 members divided into five subpopulations, with weights for crossover, mutation, and migration being set to 95, 95, and 10, respectively. GOLD allows a user-definable number of GA runs per ligand, each of which starts from a different orientation. For these experiments, the number of GA runs was set to 100 without the option of early termination, and scoring of the docked poses was performed with the original ChemPLP scoring function rescoring with ChemScore.[38] The final receptor–ligand complex for each ligand was visually inspected and chosen interactively by selecting the highest scoring pose that was consistent with experimentally-derived information about the binding mode of the ligand.

As an internal validation of the docking methodology, the crystal bound conformation of l-DADMe-ImmH was redocked into the empty catalytic pocket of the *Hs*PNP crystal structure using the same docking protocol. The conformation of the top scoring pose could reproduce the crystal structure conformation (RMSD = 0.56 Å, CHEMscore fitness = 36.8, CHEMscore $\Delta G_{bind} = -40.6$ kJ/mol), thus validating the docking methodology.

In vitro effect of 8-aminoinosine (4) on CCRF-CEM cells

Cells and reagents: CCRF-CEM cell line (ATCC® CCL-119™), a T-lymphoblast from human acute lymphoblastic leukemia, was purchased from the Rio de Janeiro Cell Bank, Brazil. Roswell Park Memorial Institute Medium (RPMI-1640), Hank's Balanced Salt Solution, fetal bovine serum (FBS), antibiotic solution (10000 U/mL penicillin, 10 mg/mL streptomycin), 3-(4,5-dimethylthiazol-2-yl)-2,5-diphenyl tetrazolium bromide (MTT) and 2′-deoxyguanosine monohydrate (dGuo) were all supplied by Sigma–Aldrich. DMSO and other reagents were of analytical grade.

Cell culture conditions: Culture medium RPMI-1640 was supplemented with 4.5 mg/mL glucose, 0.1 mg/mL penicillin, 0.14 mg/mL streptomycin and 10% inactivated FBS. Cultured cells were maintained at 37 °C in an atmosphere containing 95% air and 5% CO_2. Every 2 to 3 days cultures were centrifuged (410×g for 10 min) and subsequently resuspended in fresh medium at 3×10^5 to 1×10^6 viable cells/mL.

Measurement of cell proliferation by MTT assay: Metabolically active cells were assessed using the MTT reduction colorimetric assay, as previously reported by Mosmann.[39] Cells ($n = 4$) were seeded in 96-well plates (Corning) at density of 1×10^6 cells/mL, distributed in a total volume of 100 μL/well. CCRF-CEM cells were placed in contact with dGuo (0 or 10 μM) and 8-aminoinosine (**4**) (0 to 250 μM) for 96 hours. Stock solutions of dGuo and 8-aminoinosine (**4**) were prepared in DMSO and diluted in culture medium at 1% to obtain desired concentrations. Cell culture medium (DMSO 1%, *v*/*v*) containing or not 10 μM dGuo was used as 100% of cell viability control. Microplates were centrifuged at 410×g for 10 min. Samples were aspirated, and cells were treated with 100 μL/well of MTT solution (0.5 mg/mL in HBSS). Plates were incubated with MTT reagent at 37 °C and 5% CO_2. After 3 h of incubation, microplates were centrifuged again and MTT solution was aspirated. Cells were lysed by DMSO (100 μL/well) and cell viability was spectrophotometrically measured ($\lambda = 570$ nm), after vigorously plate mixing for 60 s, using a microplate reader (TP-Reader™, Thermoplate, Brazil). The cytotoxicity was expressed as the percentage of surviving cells in relation to respective control groups.[40]

Acknowledgements

M.C.M would like to thank the Conselho Nacional de Desenvolvimento Cientifico e Tecnológico (CNPq) and the Fundação Carlos Chagas Filho de Amparo à Pesquisa do Estado do Rio de Janeiro FAPERJ (E-26/202.909/2019).

Conflict of Interest

The authors declare no conflict of interest.

Keywords: antitumour activity · drug discovery · enzymatic assay · PNP inhibitors · screening

[1] M. Friedkin, H. M. Kalckar, *J. Biol. Chem.* **1950**, *184*, 437–448.
[2] M. L. Markert, *Immunodefic. Rev.* **1991**, *3*, 45–81.
[3] J. G. Cory, P. Chiba in *Inhibitors of Ribonucleoside Diphosphate Reductase Activity* (Eds.: J. G. Cory, A. H, Cory), Pergamon, Oxford, **1989**, pp. 245–264.
[4] S. Eriksson, L. Thelander, M. Akerman, *Biochemistry* **1979**, *18*, 2948–2952.
[5] a) J. A. Montgomery, *Med. Res. Rev.* **1993**, *13*, 209–228; b) J. C. Sircar, R. B. Gilbertsen, *Drugs Future* **1988**, *13*, 653–668; c) G. A. Omura, *Curr. Pharm. Des.* **2000**, *6*, 943–959.
[6] a) G. B. Evans, R. H. Furneaux, A. Lewandowicz, V. L. Schramm, P. C. Tyler, *J. Med. Chem.* **2003**, *46*, 3412–3423; b) V. L. Schramm, *Biochim. Biophys. Acta Mol. Basis Dis.* **2002**, *1587*, 107–117.
[7] L. L. Bennett, P. W. Allan, P. E. Noker, L. M. Rose, S. Niwas, J. A. Montgomery, M. D. Erion, *J. Pharmacol. Exp. Ther.* **1993**, *266*, 707–714.
[8] S. E. Ealick, Y. S. Babu, C. E. Bugg, M. D. Erion, W. C. Guida, J. A. Montgomery, J. A. d. Secrist, *Proc. Natl. Acad. Sci. USA* **1991**, *88*, 11540–11544.
[9] a) A. Lewandowicz, V. L. Schramm, *Biochemistry* **2004**, *43*, 1458–1468; b) E. A. Taylor, K. Clinch, P. M. Kelly, L. Li, G. B. Evans, P. C. Tyler, V. L. Schramm, *J. Am. Chem. Soc.* **2007**, *129*, 6984–6985; c) J. M. Mason, A. S. Murkin, L. Li, V. L. Schramm, G. J. Gainsford, B. W. Skelton, *J. Med. Chem.* **2008**, *51*, 5880–5884; d) A. S. Murkin, K. Clinch, J. M. Mason, P. C. Tyler, V. L. Schramm, *Bioorg. Med. Chem. Lett.* **2008**, *18*, 5900–5903.
[10] a) P. C. Kline, V. L. Schramm, *Biochemistry* **1993**, *32*, 13212–13219; b) R. W. Miles, P. C. Tyler, R. H. Furneaux, C. K. Bagdassarian, V. L. Schramm, *Biochemistry* **1998**, *37*, 8615–8621.
[11] A. Lewandowicz, E. A. T. Ringia, L.-M. Ting, K. Kim, P. C. Tyler, G. B. Evans, O. V. Zubkova, S. Mee, G. F. Painter, D. H. Lenz, *J. Biol. Chem.* **2005**, *280*, 30320–30328.
[12] a) A. Al-Kali, V. Gandhi, M. Ayoubi, M. Keating, F. Ravandi, *Future Oncol.* **2010**, *6*, 1211–1217; b) S. Mohammad, S. L. Giattino, R. T. Keenan, *Curr. Treat. Options Rheumatol.* **2015**, *1*, 143–155; c) Q.-H. Wen, L.-H. Wang, X.-A. Zeng, D.-B. Niu, M.-S. Wang, *Int. J. Biol. Macromol.* **2018**, *118*, 588–598.
[13] R. A. Copeland in *Evaluation of Enzyme Inhibitors in Drug Discovery* (Ed: R. A. Copeland), Wiley, Hoboken, **2013**, pp. 88–96.
[14] A. Bzowska, E. Kulikowska, D. Shugar, *Pharmacol. Ther.* **2000**, *88*, 349–425.
[15] M. C. de Moraes, R. G. Ducati, A. J. Donato, L. A. Basso, D. S. Santos, C. L. Cardoso, Q. B. Cass, *J. Chromatogr. A* **2012**, *1232*, 110–115.
[16] G. Cattaneo, D. Ubiali, E. Calleri, M. Rabuffetti, G. C. Hofner, K. T. Wanner, M. C. De Moraes, L. K. B. Martinelli, D. S. Santos, G. Speranza, G. Massolini, *Anal. Chim. Acta* **2016**, *943*, 89–97.
[17] J. D. Stoeckler, C. Cambor, V. Kuhns, S.-H. Chu, R. E. Parks Jr., *Biochem. Pharmacol.* **1982**, *31*, 163–171.
[18] a) D. Ubiali, C. D. Serra, I. Serra, C. F. Morelli, M. Terreni, A. M. Albertini, P. Manitto, G. Speranza, *Adv. Synth. Catal.* **2012**, *354*, 96–104; b) D. Ubiali, C. F Morelli, M. Rabuffetti, G. Cattaneo, I. Serra, T. Bavaro, A. M Albertini, G. Speranza, *Curr. Org. Chem.* **2015**, *19*, 2220–2225.
[19] A. Rinaldo-Matthis, A. S. Murkin, U. A. Ramagopal, K. Clinch, S. P. Mee, G. B. Evans, P. C. Tyler, R. H. Furneaux, S. C. Almo, V. L. Schramm, *J. Am. Chem. Soc.* **2008**, *130*, 842–844.
[20] C. Møller, M. S. Plesset, *Phys. Rev.* **1934**, *46*, 618–622.
[21] M. Alvarez-Ros, M. A. Palafox, *J. Mol. Struct.* **2013**, *1047*, 358–371.
[22] a) A. Psoda, D. Shugar, *Biochim. Biophys. Acta* **1971**, *247*, 507–513; b) G. C. Medeiros, G. J. Thomas, Jr., *Biochim. Biophys. Acta* **1971**, *238*, 1–4; c) N. Markova, V. Enchev, *J. Phys. Chem. B* **2019**, *123*, 622–630.
[23] A. R. Munns, P. Tollin, *Acta Crystallogr. Sect. B* **1970**, *26*, 1101–1113.
[24] G. A. Kicska, L. Long, H. Hörig, C. Fairchild, P. C. Tyler, R. H. Furneaux, V. L. Schramm, H. L. Kaufman, *Proc. Natl. Acad. Sci. USA* **2001**, *98*, 4593–4598.
[25] M. Huang, Y. Wang, J. Gu, J. Yang, K. Noel, B. S. Mitchell, V. L. Schramm, L. M. Graves, *Leuk. Res.* **2008**, *32*, 1268–1278.
[26] J. Elguero, C. Marzin, A. R. Katritzky, P. Linda in *The Tautomerism of Heterocycles* (Ed.: J. Elguero), Academic Press, New York, **1976**, pp. 87–102.
[27] T. Sasaki, K. Minamoto, Y. Fujiki, N. Shiomi, Y. Uda, *Nucleic Acids Symp. Ser.* **1984**, *15*, 53–56.
[28] G. Jones, P. Willett, R. C. Glen, A. R. Leach, R. Taylor, *J. Mol. Biol.* **1997**, *267*, 727–748.
[29] M. W. Schmidt, K. K. Baldridge, J. A. Boatz, S. T. Elbert, M. S. Gordon, J. H. Jensen, S. Koseki, N. Matsunaga, K. A. Nguyen, S. Su, *J. Comput. Chem.* **1993**, *14*, 1347–1363.
[30] M. D. Hanwell, D. E. Curtis, D. C. Lonie, T. Vandermeersch, E. Zurek, G. R. Hutchison, *J. Cheminformatics* **2012**, *4*, 17.
[31] F. Weigend, R. Ahlrichs, *Phys. Chem. Chem. Phys.* **2005**, *7*, 3297–3305.
[32] E. Cances, B. Mennucci, J. Tomasi, *J. Chem. Phys.* **1997**, *107*, 3032–3041.
[33] W. Sang-Aroon, V. Ruangpornvisuti, *Int. J. Quantum Chem.* **2008**, *108*, 1181–1188.
[34] H. M. Berman, T. Battistuz, T. N. Bhat, W. F. Bluhm, P. E. Bourne, K. Burkhardt, Z. Feng, G. L. Gilliland, L. Iype, S. Jain, P. Fagan, J. Marvin, D. Padilla, V. Ravichandran, B. Schneider, N. Thanki, H. Weissig, J. D. Westbrook, C. Zardecki, *Acta Crystallogr. D Biol. Crystallogr.* **2002**, *58*, 899–907.
[35] J. S. Hirschi, K. Arora, C. L. Brooks, 3rd, V. L. Schramm, *J. Phys. Chem. B* **2010**, *114*, 16263–16272.
[36] Z. Song, F. A. Kovacs, J. Wang, J. K. Denny, S. C. Shekar, J. R. Quine, T. A. Cross, *Biophys. J.* **2000**, *79*, 767–775.
[37] M. L. Verdonk, G. Chessari, J. C. Cole, M. J. Hartshorn, C. W. Murray, J. W. M. Nissink, R. D. Taylor, R. Taylor, *J. Med. Chem.* **2005**, *48*, 6504–6515.
[38] M. L. Verdonk, J. C. Cole, M. J. Hartshorn, C. W. Murray, R. D. Taylor, *Proteins* **2003**, *52*, 609–623.
[39] T. Mosmann, *J. Immunol. Methods* **1983**, *65*, 55–63.
[40] W. A. da Silva, L. C. R. P. da Silva, V. R. Campos, M. C. B. V. de Souza, V. F. Ferreira, Â. C. P. B. dos Santos, P. C. Sathler, G. S. de Almeida, F. R. F. Dias, L. M. Cabral, *Future Med. Chem.* **2018**, *10*, 527–540.

Manuscript received: November 9, 2020
Accepted manuscript online: January 6, 2021
Version of record online: February 17, 2021